J Bionic Eng 16 (2019) 311–318
DOI: https://doi.org/10.1007/s42235-019-0026-3

Journal of Bionic Engineering
http://www.springer.com/journal/42235

Effect of Solution and Calcination Time on Sol–gel Synthesis of Hydroxyapatite

Serbülent Türk[1], İbrahim Altınsoy[2], Gözde Çelebi Efe[2], Mediha Ipek[2], Mahmut Özacar[1,3], Cuma Bindal[1,2*]

1. *Biomedical*, *Magnetic and Semi Conductive Materials Research Center* (*BIMAS-RC*), *Sakarya University*, *Esentepe Campus*, *Sakarya* 54187, *Turkey*
2. *Faculty of Engineering*, *Department of Metallurgy and Materials Engineering*, *Sakarya University*, *Esentepe Campus*, *Sakarya* 54187, *Turkey*
3. *Science* & *Arts Faculty*, *Department of Chemistry*, *Sakarya University*, *Sakarya* 54187, *Turkey*

Abstract

Nano-sized hydroxyapatite (HA) particles were synthesized by sol-gel through water and ethanol based mediums of phosphoric acid (H_3PO_4) and calcium hydroxide ($Ca(OH)_2$) at pH = 11 for different calcination time (1 h, 2 h, 4 h). The effects of calcination time and solution on the crystallinity, morphology and impurity phases of the HA nanoparticles were examined *via* Fourier Transform Infrared (FTIR), Scanning Electron Microscopy (SEM), Energy Dispersive X-ray Spectroscopy (EDS) and X-ray Diffraction (XRD). It was found that crystallite size and the fraction crystallinity of the synthesized samples increased with calcination time. According to solution medium, only CaO as impurity was appeared in the water-based solvent, CaO and $Ca(OH)_2$ impurities were appeared in the ethanol-based solvent. The lowest crystallinity was 0.92 and the highest crystallinity was 1.73 respectively, depending on the process parameters. The Ca/P atomic ratio closest to the bone was found as 1.5178. As a result, the employed water-based sol-gel processes for 1 h calcination time was determined as the optimum for the formation of nano-sized HA powders using calcium hydroxide and phosphoric acid.

Keywords: bioceramics, hydroxyapatite, calcination time, XRD, sol–gel

1 Introduction

Bioceramics, such as calcium phosphates (Ca-Ps) have been widely studied for dental and orthopedic applications because they repair diseased or damaged parts of the human body and increase the quality and length of human life. Hydroxyapatite [HA, $Ca_{10}(PO_4)_6(OH)_2$] is a bioceramic material which is generally reported as bone graft for the artificial bone substitution in the biomedical field due to its good biocompatibility with the bone mineral[1]. Ceramic biomaterials that based on nano sized HA show much higher bioactivity[2,3] and improved resorbability[4,5] than micron sized ones. Release of calcium ions from nano sized HA is similar to that from natural apatite and it is essentially faster than that from coarse-grained crystals[6]. Table 1 demonstrates the most important Ca-P salts generally seen as phase impurities during the synthesis of HA particles[7].

The axis of O and Ca atoms which are parallel to the hexagonal axis with the cage constants a = 0.9418 nm and c = 0.6884 nm form the hexagonal structure of the stoichiometric HA [$Ca_{10}(PO_4)_6(OH)_2$]. Furthermore, calcium-deficient HA [CDHA, $Ca_{10-x}(PO_4)_{6-x}(HPO_4)_x(OH)_{2-x}$, $0 \le x \le 1$] is more pronounced as biological concern than stoichiometric HA because the Ca/P ratio in the bone is close to 1.5[8]. It has been claimed that CDHA, which has the structure and same chemical composition with human hard tissue, plays a significant role in various processes such as bone formation and remodeling. However, the HA mineral in bone has a CDHA structure having a Ca/P ratio that is about 1.5, which is clearly the same Ca/P ratio as the tricalcium phosphates (TCP, $Ca_3(PO_4)_2$, Ca/P = 1.5), but its chemical and structural composition is the same as the stoichiometric HA, (Ca/P = 1.67)[9].

Synthesis of HA has been carried out a few ways, which contain the conventional methods, for example, modern chemical routes (hydrothermal, emulsion, sol-gel, and co-precipitation methods) and solid-state reaction. The sol-gel process is a great deal of widespread for

***Corresponding author:** Cuma Bindal
E-mail: bindal@sakarya.edu.tr

Table 1 Ca/P atomic ratios of various calcium phosphates bioceramics[7]

Name	Symbol	Formula	Ca/P
Monocalcium phosphate monohydrate	(MCPM) and (MCPH)	$Ca(H_2PO_4)_2·H_2O$	0.5
Monocalcium phosphate anhydrous	(MCPA) and (MCP)	$Ca(H_2PO_4)_2$	0.5
Dicalcium phosphate dihydrate (Brushite)	(DCPD)	$CaHPO_4·2H_2O$	1.0
Dicalcium phosphate anhydrous (Monetite)	(DCPA) and (DCP)	$CaHPO_4$	1.0
Octacalcium phosphate	(OCP)	$Ca_8(HPO_4)_2(PO_4)_4·5H_2O$	1.33
α-Tricalcium phosphate	(α-TCP)	$Ca_3(PO_4)_2$	1.5
β-Tricalcium phosphate	(β-TCP)	$Ca_3(PO_4)_2$	1.5
Amorphous calcium phosphate	(ACP)	$Ca_x(PO_4)_y·nH_2O$	1.2–2.2
Hydroxyapatite	(HA) and (HAp)	$Ca_{10}(PO_4)_6(OH)_2$	1.67

processing of nano-structured materials among the different synthesis process. As mentioned in the previous study with microwave support[10], only starting materials are required for synthesis by sol-gel method and nano structures can be synthesized without external microwave support. The sol–gel process allows mixing of precursors which can significantly improve the chemical homogeneity of the resulting powders at the molecular level. These advantages include the relatively low synthesis temperature, high product purity, homogeneous molecular mixing and the ability to form nanosize particles and thin films[11]. Produced HA with sol–gel process has demonstrated higher bioactivity being in contrast with others, because of the presence of weakly crystalline and carbonate ions in the crystal lattice. However, studies on HA gel reproduction have always shown that the synthesis of HA is accompanied by a secondary calcium oxide (CaO) phase. As reported in literature, CaO decreases the biocompatibility of HA, therefore, there is an interest in research that attempts to overcome this problem[6,12]. For this reason attempts have been made to take away the existing calcium oxide, either through modification of the primary method, *e.g. via* the washing of the calcined powder using dilute acid solutions or increasing the aging time[12,13]. In *vitro* works, it has been shown that the bio-resorbability of the sol-gel producing HA is higher than that of conventional powder which is close to natural apatite[14].

Many methods have been utilized to produce HA, but there is little interest to research the effect of various parameters on the shape, crystallinity and the size of the nano size powder including related to sol-gel process[15]. At present study, the quality of the HA powder synthesized by the sol-gel method has been investigated by changing some parameters of the process such as mixing time, medium pH, aging time, Ca/P ratio or temperature. However, there are limited studies on the combination of calcination time and solvent parameters particularly when calcium hydroxide and phosphoric acid are used as calcium and phosphorus sources with ethanol and water based sol-gel technique, respectively. The structure of the synthesized HA powders was analyzed.

2 Experimental details

$Ca(OH)_2$ (Merck) and H_3PO_4 (Merck), which are starting calcium and phosphorous sources, were used to obtain synthesized HA under different conditions. Mixtures of the precursors were prepared taking into account a Ca/P atomic ratio similar to that of unsubstituted HA equal to 1.67. For this purpose, 1.85g $Ca(OH)_2$ calcium precursor dissolved separately in 25 mL Double Distilled Water (DDW) and 25 mL ethanol (C_2H_5OH, Sigma Aldrich) for the preparation of calcium solutions. Two separate phosphorous solutions containing 0.87 mL of H_3PO_4 were prepared according to the same procedure. Each prepared solutions were mixed in sealed containers at 60 ˚C for 30 min. The synthesis of HA was carried out in sealed containers because the content of hydroxyapatite was known to be affected by moisture in the air moisture as mentioned in the previous work[16]. The prepared calcium solutions (water and ethanol based) were added drop wise into the phosphate solutions (water and ethanol based) under stirring same condition that constant magnetic stirring for 30 minutes at 60 ˚C separately for water and ethanol based sol-gel technique. While the HA was synthesized by the sol-gel method, different pH values such as pH = 9 used in another study[17] may be used. Due to the fact that the HA

compound has OH content OH^- (as can be seen from Eq. (1)), the alkaline environment is important and the pH is adjusted to 11 in present study by using ammonium hydroxide (NH_4OH, Sigma Aldrich) for both solutions. The synthesis flow diagram was shown in Fig. 1.

The solutions were aged for 24 h at room temperature. The aged sols were exposed to thermal treatment at 105 ˚C in an air oven until the white dried gels were obtained. The dried powders were grounded in a mortar. The following equation can be used for the chemical reaction between calcium hydroxide and phosphoric acid which result in the formation of HA[6]:

$$10Ca(OH) + 6H_3PO_4 \rightarrow Ca_{10}(PO_4)_6(OH)_2 + 18H_2O. \quad (1)$$

The both dried gels were divided into three groups and were individually calcinated in oven (Nabertherm, GmbH, Germany) for 1 h, 2 h and 4 h at 950 ˚C with heating rate of 5 ˚C·min^{-1}, respectively, then placed in air for cooling to ambient temperature. Morphology of obtained powders were analyzed by X-ray Diffraction (XRD, D/Max 2200 LV), Scanning Electron Microscopy (SEM, JEOL, JMS 6060), Energy-Dispersive X-ray Spectroscopy (EDS), and Fourier Transform Infrared (FTIR, Perkin Elmer, Spectrum Two) Spectroscopy. Obtained powders were labeled as HA1–HA6. The samples labelled as HA1–HA3 were calcinated for 1 h, 2 h, and 4 h, respectively for water based solution; while other labeled samples HA4–HA6 were calcinated for 1 h, 2 h, and 4 h, respectively for ethanol based solution.

3 Results

Fig. 2 represents the morphology of the powders calcinated at 950 ˚C for 1 h, 2 h and 4 h. As observed, the HA powders obtained from both solvents were found to be non-uniform and the arrangement of cluster like particles came together to form nano-sized spherical nanoaggregates for all calcination time. However, it is possible to say that in some degree homogeneous, narrow range size and lower degree of aggregation occurred in water-based samples. As it can be seen in Fig. 3 and Table 2, EDS analysis (at ×1,000 magnification) revealed that all elements belong to HA are detected.

Fig. 4 shows X-ray diffraction patterns for the water based (a) HA1–HA3 and ethanol based (b) HA4–HA6

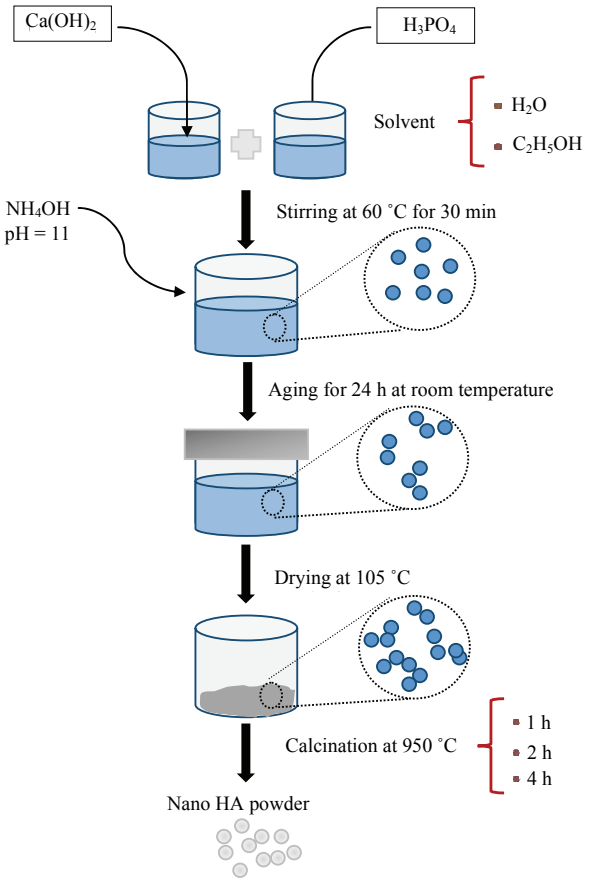

Fig. 1 Flow chart of hydroxyapatite preparation.

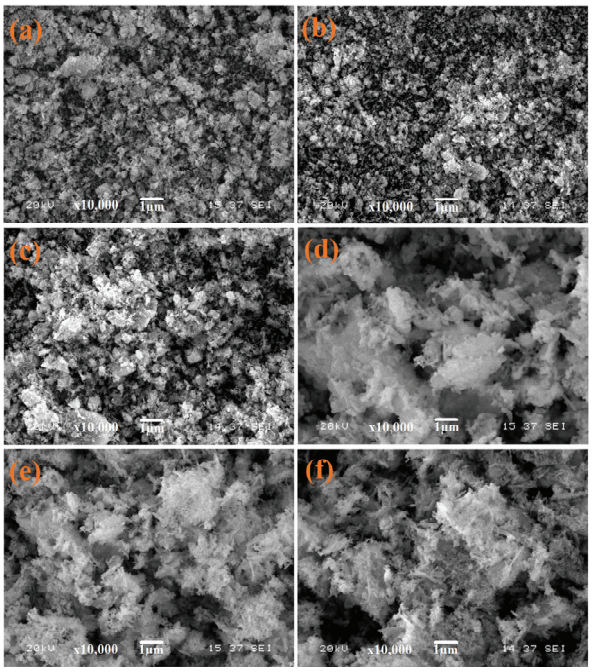

Fig. 2 SEM images of (a) HA1, (b) HA2, (c) HA3, (d) HA4, (e) HA5 and (f) HA6.

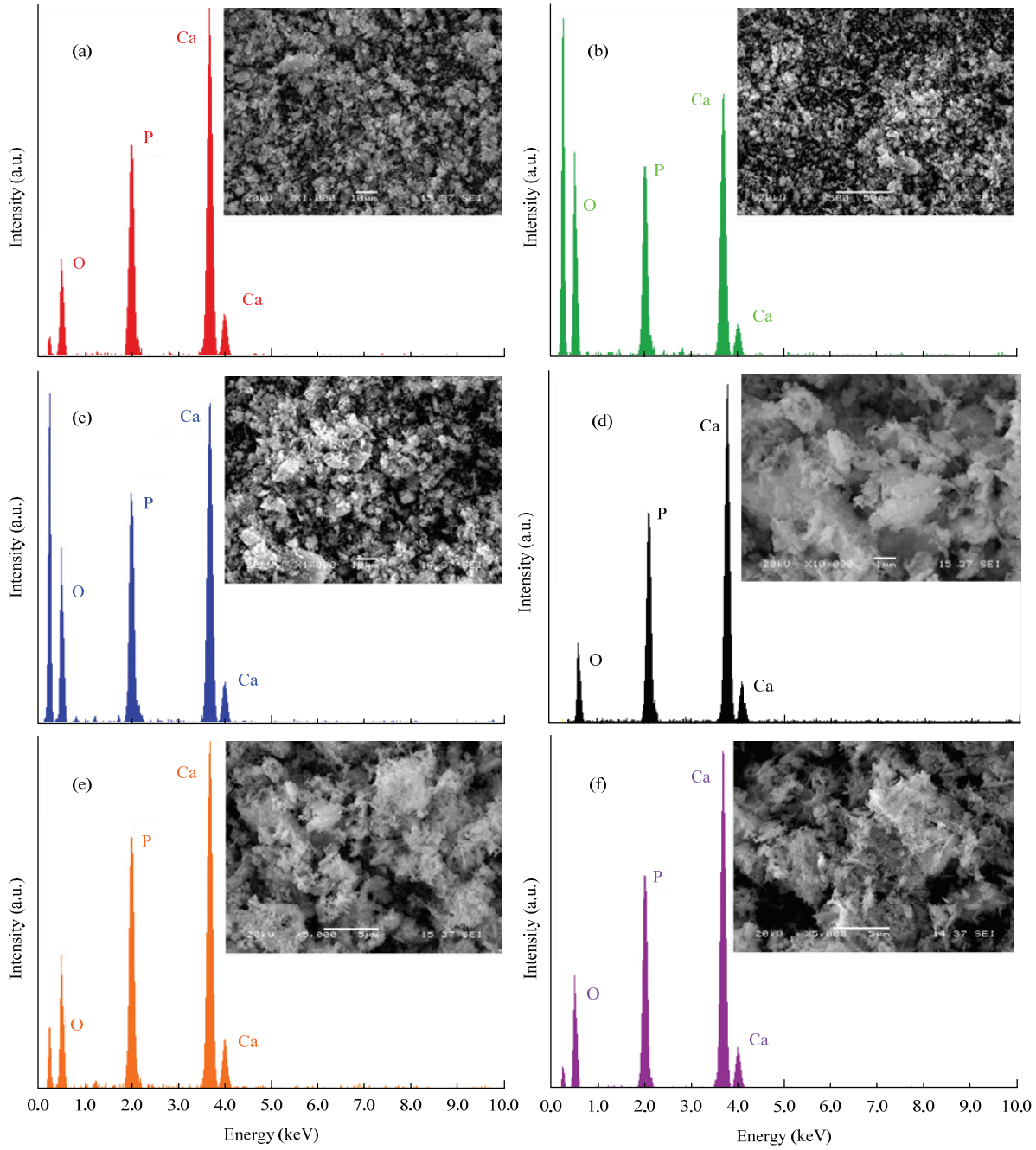

Fig. 3 EDS analyses of (a) HA1, (b) HA2, (c) HA3, (d) HA4, (e) HA5 and (f) HA6.

Table 2 EDS analysis of HA1–HA6 samples

Samples	O		P		Ca		Ca/P atomic ratio
	wt.%	at.%	wt.%	at.%	wt.%	at.%	
HA1	45.539	66.089	18.223	13.367	36.238	20.544	1.5369
HA2	58.046	75.781	15.363	10.360	26.591	13.859	1.3377
HA3	52.927	71.848	16.592	11.634	30.481	16.518	1.4198
HA4	40.623	60.9609	19.696	15.2675	39.681	23.7716	1.5570
HA5	46.273	66.106	19.401	14.317	34.326	19.577	1.3674
HA6	46.142	66.130	18.171	13.452	35.687	20.418	1.5178

powders. As observed, the formation of components such as HA, CaO and $Ca(OH)_2$ in synthesized powders was confirmed by using XRD-Rigaku D/MAX 2000 with Cu Kα radiation at 40 kV and 30 mA. The wavelength λ and step size were 0.15406 nm and 0.04°, respectively. The lattice constants were determined by least square corrections from the well-defined positions of the most intense reflections processed by the MDI Jade 6.1 software. XRD patterns showed that HA1–HA3 samples dominantly consisted of HA according to ICDD PDF card No. 86-0740 and small amount of CaO, while HA4, HA5 samples contained HA according to ICDD PDF card No. 84-1998; HA6 was HA according to ICDD PDF card No. 72-1243. Also, some CaO and $Ca(OH)_2$ were detected in HA4–HA6 samples (Fig. 4b).

The crystal size D was calculated using the equation of Debye–Scherer[18]:

$$D = \frac{k\lambda}{B_{1/2}\cos\theta}, \tag{2}$$

where k is 0.94, θ is Bragg angle of peak from diffraction and $B_{1/2}$ is the half peak width in terms of radians of the (002)hkl reflection. This reflection (002) assigns it to the plane family of Miller and demonstrates crystal growth along the c-axis of the HA crystal structure.

The fraction crystallinity, X_c, of the HA could also be determined from Ref. [19]:

$$X_c = \left(\frac{0.24}{\beta}\right)^3, \tag{3}$$

where β is the full width half maximum (FWHM) value.

The densities of the synthesized samples were obtained using the formula: $\rho = (W \times Z)/(V \times 0.6022169)$, where W is formula mass, Z is the formula units number per unit cell, and V is the volume calculated from unit cell constants[20]. The values found in the XRD patterns are shown in Table 3.

Fig. 5 illustrates the infrared spectra of the synthesized powders. The characteristic bands of internal phosphate (PO_4^{3-}) vibrations have been found in each of the all spectra. The band at 470 cm^{-1} was appoint to v_2 (O−P−O) bending vibration; the presence of two bands at 565 cm^{-1} and 607 cm^{-1} are assigned to characteristic v_4 (O−P−O) bending vibration; the 957 cm^{-1} band in the spectra was correspond to v_1 (P−O) symmetric stretching and the doublet between 1100 cm^{-1} – 1000 cm^{-1} was attributed to v_3 (P−O) antisymmetric stretching vibration.

4 Discussion

The morphologies of HA in Fig. 2 are different from each other due to high density of inter and intramolecular noncovalent hydrogen bonds between −OH groups of water molecules and nucleated HA crystalline structure. This effective interaction in Ca and P nucleation decreased the crystal growth compared to ethanol. Thus, it causes decrease in aggregation. On the contrary, the density of intermolecular hydrogen bonding interactions in the alcohol is less dense than in the water. Therefore, the intermolecular hydrogen bonding interactions between HA crystalline structures were more dominant than in the water and it caused an increase in aggregation. Also according to EDS analysis results (Table 2) HA1, HA4 and HA6 samples were found to be closest HA in bone structure which is 1.5.

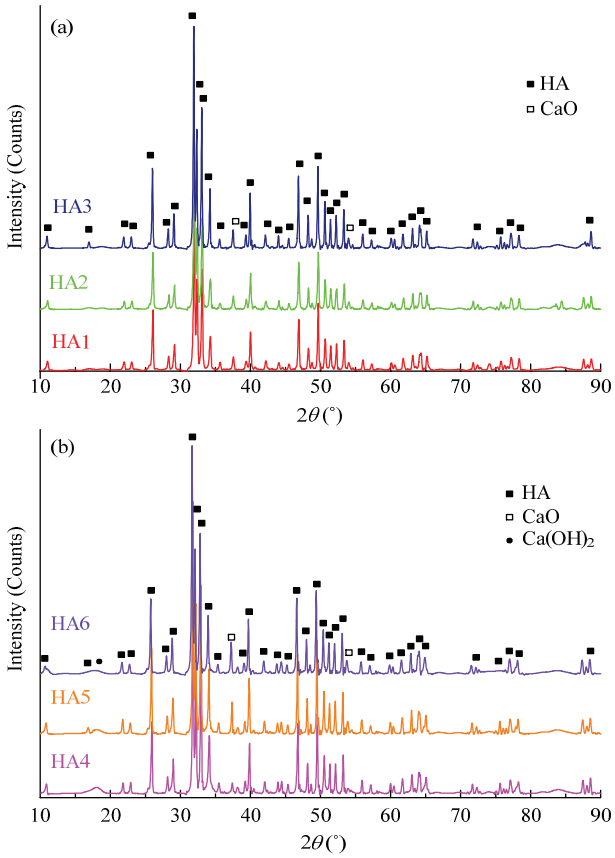

Fig. 4 X-ray diffraction patterns for the water based (a) HA1–HA3 and ethanol based (b) HA4–HA6 powders.

Table 3 Lattice parameters and crystallite sizes of HA1–HA6 reflected by XRD pattern

Samples	Space group	Lattice constants (Å)			Line width (0 0 2) FWHM (°)	2θ (°)	Z	Density, ρ (g·cm^{-3})	Average crystal size, D (nm)	Fraction crystallinity, X_c
		a	b	c						
HA1	$P6_3 \cdot m^{-1}$ (176)	9.352	9.352	6.882	0.247	26.099	2	3.2	34.5	0.92
HA2	$P6_3 \cdot m^{-1}$ (176)	9.352	9.352	6.882	0.222	26.101	2	3.2	38.38	1.26
HA3	$P6_3 \cdot m^{-1}$ (176)	9.352	9.352	6.882	0.201	26.022	2	3.2	42.39	1.70
HA4	$P6_3 \cdot m^{-1}$ (176)	9.417	9.417	6.874	0.226	25.941	2	3.159	37.69	1.20
HA5	$P6_3 \cdot m^{-1}$ (176)	9.417	9.417	6.874	0.216	25.882	2	3.159	39.43	1.37
HA6	$P6_3 \cdot m^{-1}$ (176)	9.432	9.432	6.881	0.200	25.798	1	3.146	42.58	1.73

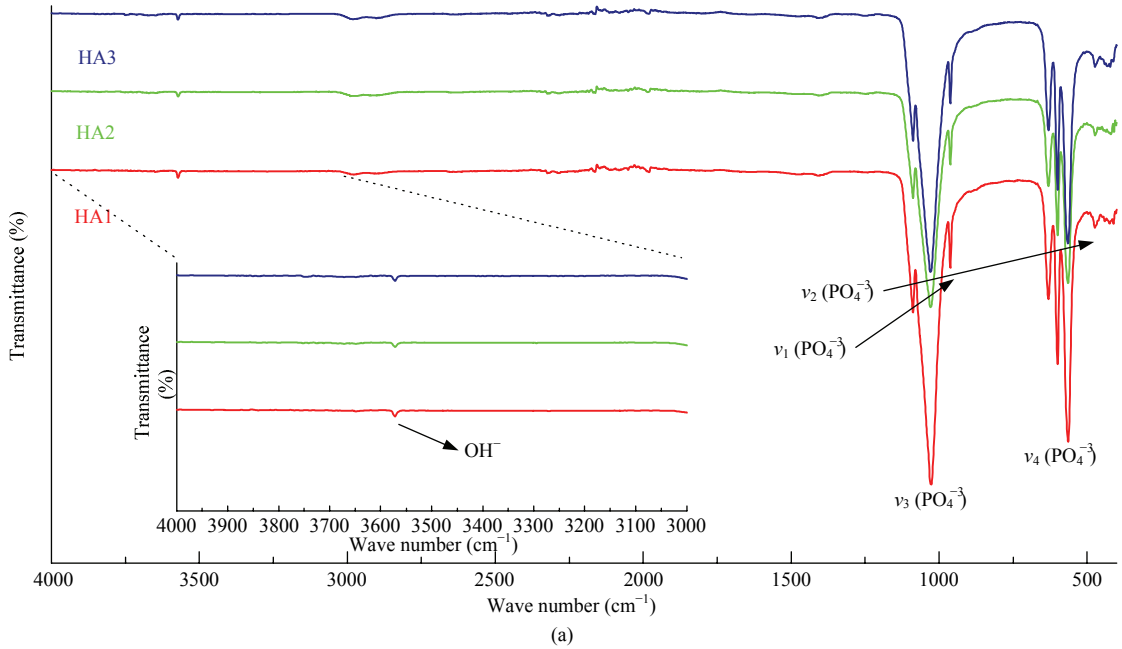

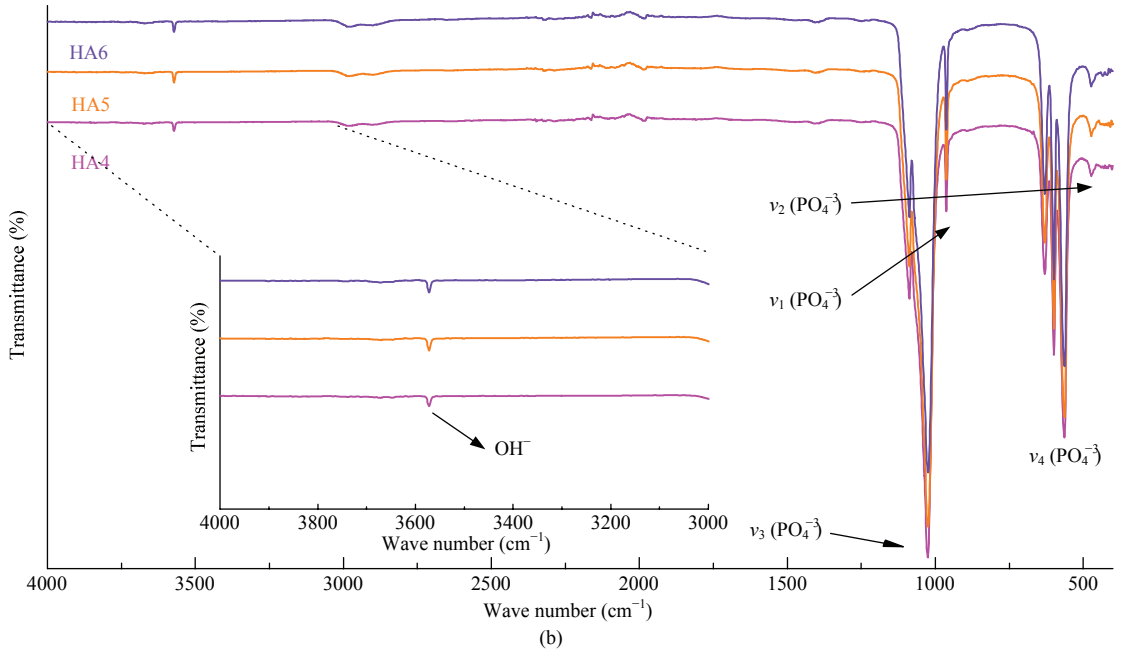

Fig. 5 FTIR spectra of (a) HA1–HA3 and (b) HA4–HA6.

XRD results for water and alcohol based samples according to the calcination time of 1 h, 2 h and 4 h were shown in Fig. 4. These patterns indicate HA is the dominant phase, nevertheless some CaO and $Ca(OH)_2$ contributions were observed. The presence of CaO (ICDD PDF card No. 48-1467) has been reported from XRD patterns of both water (Fig. 4a) and ethanol based (Fig. 4b) powders. Also the presence of $Ca(OH)_2$ (ICDD PDF card No. 44-1481) has been indicated from XRD patterns of ethanol based powders. When calcination time increases; while no increase or decrease in HA peaks, peak intensity of other phase changed. The weakest CaO peaks were found at 1 h calcination time in alcohol-based samples as in water-based samples. Thus, the impurity peaks [CaO peak (002) at 2θ = 37.3 and $Ca(OH)_2$ peak (001) at 2θ = 18.1] were found to be increased with calcination time in both water and alcohol based samples. This showed that HA decomposes with the increase in calcination time and thus CaOH and CaO peaks formed.

It is possible to claim that both the crystallite size and fraction crystallinity increase with the calcination temperature. HA with high crystallinity exhibits little or no activity for bio-resorption[21,22] and forms the smooth surface and regular shape of the nanoparticles[23].

The evaluated degrees of crystallinity for these samples are given in Table 3. The crystallinity increased in the range of 0.92 – 1.70 and 1.20 – 1.73 for the HA powders prepared in water and alcohol based solution, respectively, which indicated a strong calcination temperature and solution medium dependence of the crystallinity of the HA prepared. It was noticed that the crystallinity was increased in direct proportion to the calcination time in both HA samples. However, the lowest crystallinity was observed in HA1, which was synthesized in water based medium and calcined for 1 h. The reason is probably that the calcination time also affects the morphology and thus the crystallinity as reported by previous study[24]. There was no significant change in crystallinity when compared to solution media.

The obtained FTIR vibration bands demonstrate the characteristic molecular structures of the poly-hedrons of PO_4^{3-} in the lattice of apatite[25,26]. The peak at 3738 cm^{-1} observed in four spectra corresponds to the tensile vibration of the OH^{-1} ions in the HA lattice[27]. Therefore, FTIR spectra support the XRD results.

5 Conclusion

HA samples were synthesized successfully in both aqueous and alcoholic solutions with different process parameters. The lowest crystallinity was found as 0.92 in the HA2 sample, while the highest crystallinity was found in the HA6 sample as 1.73. And also, the Ca/P atomic ratio closest to the bone was found as 1.5178 in the HA6 sample. After the synthesis process, dominant HA phase along with small amount of CaO and $Ca(OH)_2$ were obtained depending on solvent media and calcination time. According to process parameters, calcination time strongly determines the purity of HA compound dominantly obtained in water based solution with small amount of CaO. Consequently, water based solvent and 1 h calcination time at 950 ˚C process were found to be optimal for the synthesis of HA at pH = 11 with calcium hydroxide and phosphoric acid sources compared to ethanol solution.

References

[1] Gopi D, Kavitha L, Rajeswari D. Synthesis of pure and substituted hydroxyapatite nanoparticles by cost effective facile methods, In Aliofkhazraei M ed., *Handbook of Nanoparticles*, 2015, 167–190.

[2] Cai Y R, Liu Y K, Yan W Q, Hu Q H, Tao J H, Zhang M, Shi Z L, Tang R K. Role of hydroxyapatite nanoparticle size in bone cell proliferation. *Journal of Materials Chemistry*, 2007, **17**, 3780–3787.

[3] Dorozhkin S V. Nanosized and nanocrystalline calcium orthophosphates. *Acta Biomaterialia*, 2010, **6**, 715–734.

[4] Dong Z H, Li Y B, Zou Q. Degradation and biocompatibility of porous nano-hydroxyapatite/polyurethane composite scaffold for bone tissue engineering. *Applied Surface Science*, 2009, **255**, 6087–6091.

[5] Wang Y Y, Liu L, Guo S R. Characterization of biodegradable and cytocompatible nano-hydroxyapatite/polycaprolactone porous scaffolds in degradation *in vitro*. *Polymer Degradation and Stability*, 2010, **95**, 207–213.

[6] Sadat-Shojai M, Khorasani M T, Dinpanah-Khoshdargi E, Jamshidi A. Synthesis methods for nanosized hydroxyapatite with diverse structures, *Acta Biomaterialia*, 2013, **9**, 7591–7621.

[7] Vallet-Regí M, González-Calbet J M. Calcium phosphates as substitution of bone tissues. *Progress in Solid State Chem-*

istry, 2004, **32**, 1–31.

[8] Liu D M, Troczynski T, Tseng W J. Water-based sol–gel synthesis of hydroxyapatite: Process development. *Scanning Electron Microscopy*, 2001, **22**, 1721–1730.

[9] Liou S C, Chen S Y, Lee H Y, Bow J S. Structural characterization of nano-sized calcium deficient apatite powders. *Biomaterials*, 2004, **25**, 189–196.

[10] Türk S, Altınsoy İ, ÇelebiEfe G, Ipek M, Özacar M, Bindal C. Microwave–assisted biomimetic synthesis of hydroxyapatite using different sources of calcium. *Materials Science and Engineering*: *C*, 2017, **76**, 528–535.

[11] Bose S, Saha S. Synthesis of hydroxyapatite nanopowders via sucrose-templated sol-gel method. *Journal of the American Ceramic Society*, 2003, **86**, 1055–1057.

[12] Eshtiagh-Hosseini H, Housaindokht M R, Chahkandi M. Effects of parameters of sol-gel process on the phase evolution of sol–gel-derived hydroxyapatite. *Materials Chemistry and Physics*, 2007, **106**, 310–316.

[13] Hsieh M F, Perng L H, Chin T S, Perng H G. Phase purity of sol–gel–derived hydroxyapatite ceramic. *Biomaterials*, 2001, **22**, 2601–2607.

[14] Fathi M H, Hanifi A, Mortazavi V. Preparation and bioactivity evaluation of bone-like hydroxyapatite nanopowder. *Journal of Materials Processing Technology*, 2008, **202**, 536–542.

[15] Michael F M, Khalid M, Ratnam C T, Chee C Y, Rashmi W, Hoque M E. Sono-synthesis of nanohydroxyapatite: Effects of process parameters. *Ceramics International*, 2015, **42**, 6263–6272.

[16] Waheed S, Sultan M, Jamil T, Hussain T. Comparative analysis of hydroxyapatite synthesized by sol–gel, ultrasonication and microwave assisted technique. *Materials Today: Proceedings*, 2015, **2**, 5477–5484.

[17] Bakan F, Laçin O, Sarac H. A novel low temperature sol–gel synthesis process for thermally stable nano crystalline hydroxyapatite. *Powder Technology*, 2013, **233**, 295–302.

[18] Huang Z, Zhou Q, Wang X F, Liu Z C. A biomimetic synthesis process for Sr^{2+}, HPO_4^{2-}, and CO_3^{2-} substituted nanohydroxyapatite. *Materials and Manufacturing Processes*, 2016, **31**, 217–222.

[19] Degirmenbasi N, Kalyon D M, Birinci E. Biocomposites of nanohydroxyapatite with collagen and poly(vinyl alcohol). *Colloids Surfaces B*: *Biointerfaces*, 2006, **48**, 42–49.

[20] Fan W, Sun Z, Wang J, Zhou J, Wu K, Cheng Y. Evaluation of $Sm_{0.95}Ba_{0.05}Fe_{0.95}Ru_{0.05}O_3$ as a potential cathode material for solid oxide fuel cells. *RSC Advances*, 2016, **6**, 34564–34573.

[21] Sanosh K P, Chu M C, Balakrishnan A, Lee Y J, Kim T N, Cho S J. Synthesis of nano hydroxyapatite powder that simulate teeth particle morphology and composition. *Current Applied Physics*, 2009, **9**, 1459–1462.

[22] Currey J. Sacrificial bonds heal bone. *Nature*, 2001, **414**, 699.

[23] Pang Y X, Bao X. Influence of temperature, ripening time and calcination on the morphology and crystallinity of hydroxyapatite nanoparticles. *Journal of the European Ceramic Society*, 2003, **23**, 1697–1704.

[24] Chen L, Tang C Y, Ku H S, Tsui C P, Chen X. Microwave sintering and characterization of polypropylene/multi-walled carbon nanotube/hydroxyapatite composites. *Composites Part B*: *Engineering*, 2014, **56**, 504–511.

[25] Paz A, Guadarrama D, López M, González J E, Brizuela N, Aragón J. A comparative study of hydroxyapatite nanoparticles synthesized by different routes. *Química Nova*, 2012, **35**, 1724–1727.

[26] Varma H K, Babu S S. Synthesis of calcium phosphate bioceramics by citrate gel pyrolysis method. *Ceramics International*, 2005, **31**, 109–114.

[27] Mujahid M, Sarfraz S, Amin S, Road J. On the formation of hydroxyapatite nano crystals prepared using cationic surfactant. *Materials Research-Ibero-American Journal of Materials*, 2015, **18**, 468–472.